CARBON 93 (2015) 1–10

Available at www.sciencedirect.com

ScienceDirect

journal homepage: www.elsevier.com/locate/carbon

Low-energy excitations of graphene on Ru(0001)

D. Maccariello [a,b], D. Campi [c], A. Al Taleb [b], G. Benedek [c,d], D. Farías [b,e,f,*], M. Bernasconi [c], R. Miranda [a,b,e,f]

[a] Instituto Madrileño de Estudios Avanzados en Nanociencia (IMDEA-Nanociencia), 28049 Madrid, Spain
[b] Departamento de Física de la Materia Condensada, Universidad Autónoma de Madrid, 28049 Madrid, Spain
[c] Dipartimento di Scienza dei Materiali, Universita di Milano-Bicocca, Via Roberto Cozzi 55, 20125 Milano, Italy
[d] Donostia International Physics Center (DIPC), University of the Basque Country (EHU-UPV), Paseo Manuel de Lardizbal 4, 20018 Donostia/San Sebastián, Spain
[e] Instituto de Ciencia de Materiales "Nicolás Cabrera", Universidad Autónoma de Madrid, 28049 Madrid, Spain
[f] Condensed Matter Physics Center (IFIMAC), Universidad Autónoma de Madrid, 28049 Madrid, Spain

ARTICLE INFO

Article history:
Received 13 March 2015
Accepted 8 May 2015
Available online 15 May 2015

ABSTRACT

The structure and the acoustic phonon branches of graphene on Ru(0001) have been experimentally investigated with helium atom scattering (HAS) and analyzed by means of density functional theory (DFT) including Grimme dispersion forces. In-plane interactions are unaffected by the interaction with the substrate. The energy of 16 meV for the vertical rigid vibration of graphene against the Ru(0001) surface layer indicates an interlayer effective force constant about five times larger than in graphite. The Rayleigh mode observed for graphene/Ru(0001) is almost identical to the one measured on clean Ru(0001). This is accounted for by the strong bonding to the substrate, which also explains the previously reported high reflectivity to He atoms of this system. Finally, we report the observation of an additional acoustic branch, closely corresponding to the one already observed by HAS in graphite, which cannot be ascribed to any phonon mode and suggests a possible plasmonic origin.

1. Introduction

Phonon dispersion curves are extremely sensitive to interatomic forces of adsorbed layers, including the interaction between adlayer and substrate atoms. The system formed by graphene on transition metal surfaces provides a good example of how small changes in the strength of the graphene–substrate interaction modify the corresponding phonon dispersion curves [1]. The graphene/Ni(111) system, for instance, is characterized by graphite-like phonon modes, softened due to the interaction of graphene with the substrate [2]. This softening is removed after intercalation of Ag or Cu below the graphene layer, rendering surface phonon dispersion curves which are very similar to those of graphite [3,4]. Calculations of the surface phonon dispersion based on a force constant model revealed that the force constants for the graphene/Cu interface are comparable to those of pristine graphite [5,6]. However, these and similar studies were limited to phonon energies above 40 meV, and therefore did not allow to follow the dispersion of the acoustical modes down to the center of the Brillouin zone. This information is relevant, since thermal conductivity of graphene near room

* *Corresponding author at:* Departamento de Física de la Materia Condensada, Universidad Autónoma de Madrid, 28049 Madrid, Spain. E-mail address: daniel.farias@uam.es (D. Farías).
http://dx.doi.org/10.1016/j.carbon.2015.05.028
0008-6223/

temperature is dominated by contributions from acoustic phonons [7,8]. For graphene on SiO_2, recent molecular dynamics simulations have shown that increasing the strength of the graphene–substrate interaction enhances the thermal conductivity of supported graphene. Such enhancement is due to the coupling of graphene ZA modes to the substrate Rayleigh waves [9]. For the case of stronger graphene–substrate interaction, hybridization of the low-energy graphene flexural mode with the Rayleigh wave of the substrate is expected to occur [10], as reported for graphene/TaC(111) [11].

The energy range of graphene acoustic vibrations, their dispersion and their modifications due to the interaction with the metal substrate fall in the range easily accessible to Helium Atom Scattering (HAS). Because of the low energies employed (10–100 meV), neutral He atoms probe the topmost surface layer of any material in an inert, completely non-destructive manner [12]. Moreover, HAS diffraction provides an accurate description of the surface charge density at the Fermi level, more specifically of its corrugation as seen by He atoms at thermal energies, to be compared with the crystallographic corrugation of atomic positions measured with electronic probes.

In the present work, we report a HAS study of the phonon dynamics of graphene grown on Ru(0001). This system is especially interesting, since it is an excellent candidate to be used as a focusing mirror in scanning He atom microscopy [13]. A very high surface reflectivity to He atoms has been reported (23%) [14,15], which is surprising for a layer made of C atoms. Our current study provides a sound explanation for this fact, based on the low-energy phonon dynamics of this system. The corresponding inelastic HAS spectra are characterized by a comparatively strong intensity from the Ru(0001) Rayleigh wave (RW) and small intensities from the flexural (ZA) and longitudinal (LA) phonon branches in the acoustic region, and from an unexpected third acoustic branch of probable electronic origin. The large scattering intensity from ruthenium RW is surprising, since Ru atoms are completely screened out by the graphene sheet, though compatible with the small surface charge density modulation induced by the exclusive motion of Ru substrate atoms. All this concurs to indicate a high flexibility of graphene at small wavevectors, which allows it to adapt to the instantaneous substrate profile, explaining the observed extraordinarily high specular reflectivities for He [15].

The simulation of the HAS diffraction pattern derived from Density Functional Theory (DFT) with the inclusion of dispersion forces is seen to reproduce experiment quite well, including the moiré satellite peaks. The electron density corrugation as determined by HAS turns out to be appreciably smaller than the atomic one [17], indicating that the charge redistribution tends to smooth out the long-period corrugation of the graphite sheet induced by the ruthenium substrate.

2. Experimental

The experiments were performed with a high resolution He atom scattering (HAS) time-of-flight (TOF) spectrometer, described in detail elsewhere [18,19]. Essentially, the He atom beam, produced in a high pressure free jet expansion of the gas, is modulated by a rotating disk chopper for TOF measurements. The helium atoms scattered from the sample, after travelling trough three differentially pumped stages along the 1.7 m long drift tube, are detected by means of a mass sensitive detector. The angle between incident and scattered beam, in a planar geometry, is fixed at a total angle $\theta_{SD} = \theta_i + \theta_f = 105.4^\circ$. The energy of the incident beam can be continuously varied in a range from 20 to 80 meV by controlling the temperature of the nozzle. The angular distributions were measured by rotating the crystal by an angle θ_i around a normal to the plane defined by the incident and the outgoing beams. The dynamical study was done by recording TOF spectra over a wide range of incident angles, in order to get the surface phonon dispersion along the $\overline{\Gamma}\overline{M}$ direction of the first Brillouin zone (IBZ) of either graphene or Ru(0001). The results collected for a single graphene monolayer on a Ru(0001) substrate were first compared with an early study of the clean substrate surface [20].

An atomically clean, bulk C depleted, Ru(0001) substrate was prepared by standard sputtering-annealing cycles, followed by oxygen exposure at 1150 K and final flash to 1500 K. A high quality graphene monolayer was epitaxially grown on Ru(0001) by thermal decomposition of ethylene at 1150 K [14,16,17]. The cleanliness and azimuthal alignment of the sample have been monitored by means of the analysis of HAS angular distributions, as well as by low electron energy diffraction (LEED).

2.1. *Structural properties*

Due to the moiré reconstruction, the HAS diffraction pattern from the Gr/Ru(0001) surface shows a more complex structure than the diffraction patterns from lattices with single periodicity. Fig. 1 shows a high-resolution HAS pattern measured from a Gr/Ru(0001) sample. The angular distribution has been normalized to the intensity of the specular peak. This spectrum (shown in logarithmic scale) was collected with the temperature of the sample and nozzle at $T_S = 150$ K, which corresponds to an incident energy of the He beam $E_i = 33$ meV. The specular peak is very sharp, with a FWHM $= 0.15^\circ$. This corresponds roughly to the angular resolution of the instrument, revealing the extremely high surface quality of the sample. The (1,0) diffraction peak of the graphene atomic lattice (labelled as Gr(1,0)) is observed at an incident angle $\theta_i = 25.4^\circ$. Several additional diffraction peaks can be clearly seen in the spectrum, close to the maxima of the specular peak ($\theta_i = 52.7^\circ$) and at lower incident angles, nearby the Gr(1,0) peak. These reveal the long-period superstructure of the ordered moiré reconstruction. The clear peaks appearing at $\theta_i = 50.6^\circ$ and $\theta_i = 54.8^\circ$ (in proximity of the specular peak) correspond to the first order diffraction of the graphene moiré. Note that the high order Bragg peaks are clearly detected, i.e. m(10,0) up to m(13,0), which also confirms the excellent quality of the graphene samples. The diffraction spectra show that, along this azimuthal direction, the periodicity of the moiré superstructure is twelve times larger than the atomic periodicity of graphene. Therefore, the m(12,0) and Gr(1,0) diffraction peaks appear at the same angular position.

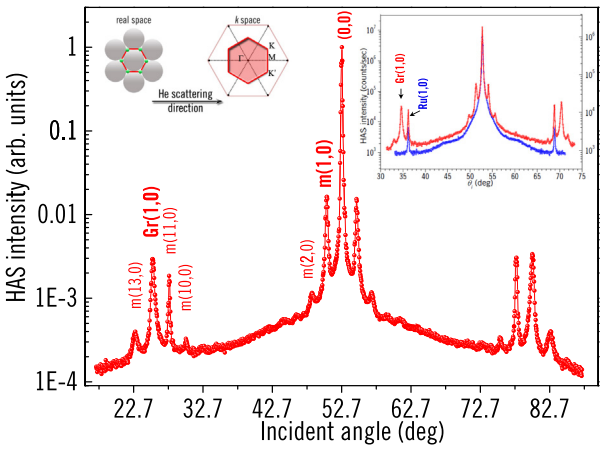

Fig. 1 – Angular distribution of He scattering from the Gr/Ru(0001) surface along the $\overline{\Gamma}\overline{M}$ direction. The incident beam energy is $E_i = 16.5$ meV and the surface temperature is 150 K. The diffraction peaks of the moiré structure are also indicated. Inset: Angular distribution from the Ru(0001) (blue curve, left scale) and graphene (red curve, right scale) surfaces measured at $E_i = 30$ meV. Also shown is the He beam orientation with respect to the $[1\bar{1}00]$ azimuthal direction of the *hcp* Ru(0001) (gray spheres). The picture of an atop lying graphene is highlighted by the red hexagon. (A colour version of this figure can be viewed online.)

The inset of Fig. 1 shows a comparison of angular distributions from the surfaces of the clean Ru substrate and the Gr/Ru(0001) sample. The spectra have been shifted to allow a better comparison of the intensities. Sharp diffraction peaks indicate a well-ordered Ru(0001) surface. The spectrum of Ru(0001) (blue line) along the $[1\bar{1}00]$ azimuthal direction, exhibits only the first order diffraction peaks, in agreement with previous work [20,27]. The moiré $m(11,0)$ peak of the graphene covered sample coincides with the first order diffraction peak of the Ru(0001) substrate. An interesting result from this comparison is the high intensity of this peak, in spite of the fact that the Ru substrate is completely covered by the graphene monolayer. Moreover, the peak preserves roughly the same intensity and sharpness (FWHM $\approx 0.2°$) than for the clean Ru(0001) surface.

2.2. *Time-of-flight spectra*

Fig. 2 shows representative TOF spectra taken at different incident conditions. Peaks corresponding to the different phonon modes are labeled. The diffuse elastic peak has been employed to set the zero in the energy transfer scale and to monitor the quality of the surface. The intensity of the diffuse elastic peak as compared to the specular one and its sharpness (FWHM ≈ 0.5 meV) denote the good quality of the samples. The measurements in Fig. 2 were collected for incident angles larger than the specular angle where annihilation processes mostly occur within the first Brillouin zone and are therefore dominant. Series of inelastic HAS spectra for different incident angles have been taken for various values of the incident energy, ranging from 21 to 67 meV, and the surface temperature (from 120 K to room temperature), so as to explore the acoustic phonon dispersion curves of graphene/Ru(0001) as extensively as possible.

Fig. 3 shows the data points corresponding to the surface phonon dispersion curves along the $\overline{\Gamma}\overline{M}$ direction of the BZ

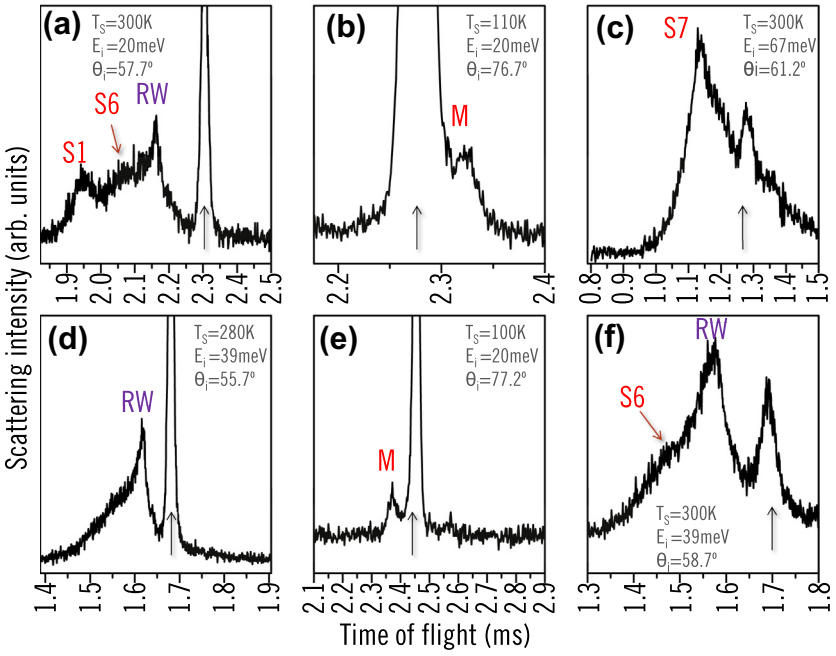

Fig. 2 – Time-of-flight spectra taken along the $\overline{\Gamma}\overline{M}$ direction of Gr/Ru(0001), at different experimental conditions. The arrows indicate the position of the diffuse elastic peak, taken as zero of the energy scale. Peaks S1, S6, and S7 correspond to the three surface modes already reported for graphite [30]; RW corresponds to the Rayleigh wave, and M to a low energy phonon mode. (A colour version of this figure can be viewed online.)

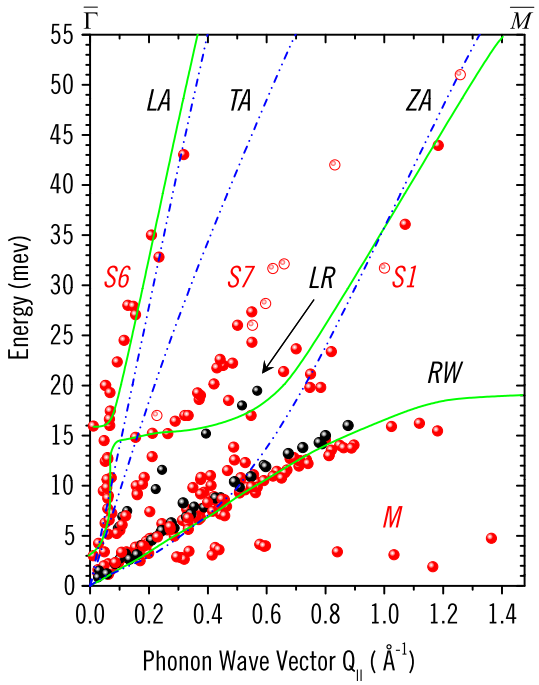

Fig. 3 – Surface phonon dispersion along $\overline{\Gamma}\overline{M}$ of Gr/Ru(0001) (red spheres) and clean Ru(0001) substrate (black spheres). Open circles represent less-clear peaks in the TOF spectra. The blue dotted lines represent the graphene modes obtained from DFT calculations [28]. Solid green lines correspond to a fit using a double linear chain model (see text). The modes observed are the longitudinal acoustical mode (LA or S6), the perpendicular acoustical (ZA or S1) and the Rayleigh wave (RW). The S7 mode is assigned to an electronic origin. For an interpretation of the mode labelled with M (see text). The longitudinal resonance (LR) is observed only in the clean Ru(0001) surface. (A colour version of this figure can be viewed online.)

for Gr/Ru(0001) (red circles) and for the clean Ru(0001) surface (black circles). The data points have been obtained applying to the measured TOF spectra the corresponding scan curve [29]. For comparison, the modes reported in previous DFT calculations for free-standing graphene [28] are also shown (blue dash-dotted lines). The present experimental data for the clean Ru(0001) surface include the Rayleigh wave (RW) branch and the longitudinal resonance (LR) mode, which is peculiar to all metal surfaces. Our data are in excellent agreement with previous HAS data measured by Braun et al. [20] (not shown).

2.3. *Dispersion curves*

The two steeper acoustic phonon branches observed with HAS, attributed to polarizations parallel to the surface and referred to as the longitudinal acoustic (LA or S6) and shear-horizontal (SH or S7) surface modes, reproduce very well those originally measured with HAS for graphite (0001) surface along the same direction (not shown) [30]. This means that the interaction of graphene with the Ru substrate, which largely exceeds the interlayer interaction in graphite, leaves practically unchanged the in-plane interactions, despite the periodic corrugation of the graphene sheet. It should be noted that the S7 branch is too soft with respect to the SH branch known for bulk graphite, just as much as for the (0001) surface of graphite [30], so that the attribution to the SH branch remains questionable and an alternative explanation needs to be discussed below. The major difference between supported graphene and graphite concerns however the S1 branch, which corresponds to the acoustic ZA branch in graphite and free-standing graphene, but does not go to zero for $Q_{\parallel} \to 0$ due to the Gr–Ru interplanar force constants. However, for $Q_{\parallel} \to \overline{M}$ also the S1 branch approaches the corresponding ZA branch of self-standing graphene, as expected for the growing, finally over-whelming importance of graphene in-plane force constants. Also the validity of this limit is related to the negligible modification of graphene in-plane force constants induced by Ru.

The lowest observed acoustic branch vanishing for $Q_{\parallel} \to 0$, corresponding to the RW mode is almost identical to the one measured on the clean Ru(0001) substrate. This is a quite surprising result, since graphene is completely covering the surface. Given the fact that He atoms are scattered by the surface electrons where their density is of the order of 10^{-4} a.u., the large inelastic intensity from Ru(0001) RW would suggest that the Ru surface contributes a substantial amount of charge at the Fermi level which extends far beyond the graphene layer. The question is whether this mode is visible due to an induced charge density oscillation through the so called "quantum sonar" effect [31] or if the graphene layer is so flexible to follow the motion of the underlying Ru substrate. The fact that for wavevectors approaching the zone boundary the ZA frequency becomes much stiffer than that of the RW indicates that the flexibility of the graphene sheet becomes negligible, thus favoring the quantum sonar effect. The DFT analysis presented below confirms this mechanism.

3. Theory

3.1. *Computational details*

The reconstruction of graphene on ruthenium is approximated by 12×12 cells of carbon atoms commensurate with an 11×11 supercell of Ru in its (0001) surface plane. In the present ab initio calculations a minimal slab of three Ru layers with the graphene adsorbed on a single side was used. The slab was separated by its periodic replicas in the z-direction by a vacuum region 12 Å wide. Calculations were performed within the framework of DFT with both the local density approximation (LDA) for the exchange–correlation functional and the PBE generalized gradient approximation [21] corrected with a semi-empirical Van der Waals interaction [Grimme2010 DFT-D3] as implemented in the Quantum-Espresso suite of programs [22]. We used ultrasoft pseudopotentials [23] with the semi-core d electrons included for ruthenium. The Kohn–Sham states were expanded in plane waves up to 30 Ry cutoff, while a 300 Ry cutoff has been used for the charge density. Only the $\overline{\Gamma}$-point was used to sample the Brillouin zone and a smearing of 0.01 Ry was introduced

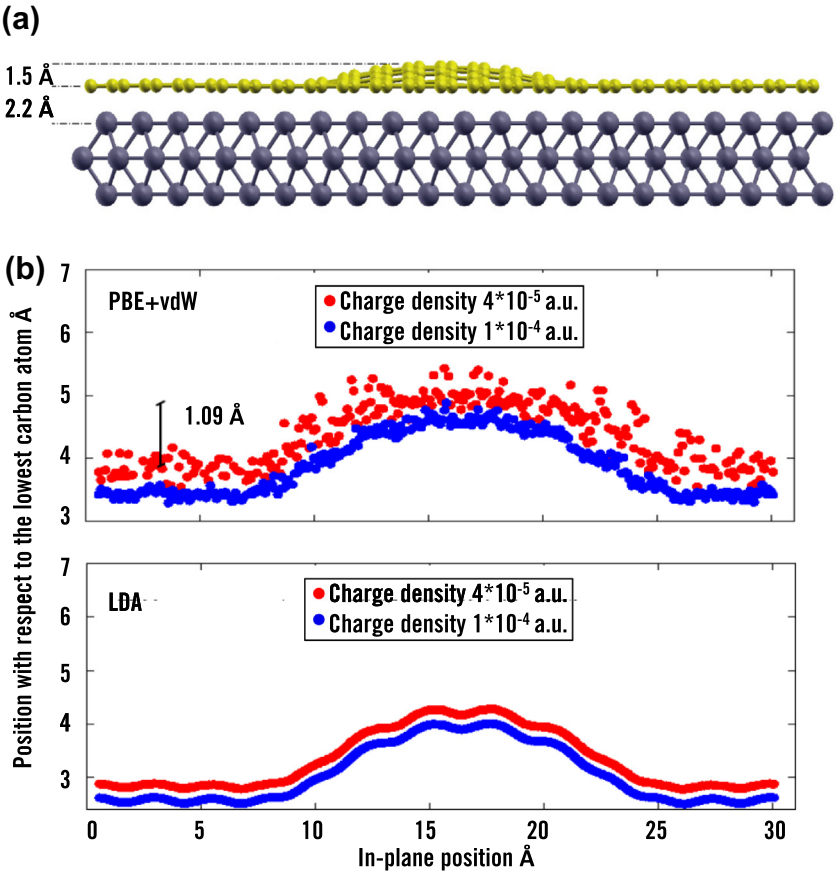

Fig. 4 – (a) Equilibrium structure of Gr/Ru(0001). (b) Charge density profile across the cell center calculated with PBE + Grimme approximation (PBEGA) and local density approximation (LDA). (A colour version of this figure can be viewed online.)

in the electronic occupation to deal with the metallic character of ruthenium and graphene. To compute the equilibrium configuration we started with a flat graphene sheet, and relaxed the structure until the forces were below 10^{-4} a.u.

3.2. *Structural properties*

The structure of the graphene layer obtained from the DFT calculations is shown in Fig. 4. After the relaxation with the PBE + Grimme functional the graphene sheet exhibited a geometrical corrugation of 1.15 Å and a minimum distance form the Ru surface of 2.2 Å. These results are consistent with previous [24] and the most recent ab initio calculations performed with a larger supercell (25×25 C on 23×23 Ru) [25]. Also the bond distribution obtained in this work for the $(12 \times 12 - 11 \times 11)$ configuration (Fig. 5) is similar to that reported in Ref. [25]. The calculated bi-modal bond distribution clearly shows the two zones characterizing the structure of graphene/Ru(0001): the strongly interacting flat region closer to the substrate, where the bonds are stretched in order to adjust as much as possible to ruthenium periodicity, and a weakly interacting region, more distant from the substrate in the upper part of the nanodome where the bonds are much less distorted and roughly correspond to the value of the ideal graphene sheet. This explains the observation of first order diffraction peaks from graphene, labeled as Gr(1,0) in Fig. 1.

The LDA functional yields a larger atomic corrugation of 1.4 Å and a corresponding smaller distance from the substrate of 2.1 Å. Since the PBE + Grimme approximation (PBEGA) is known to give better results for this system, the structure obtained with LDA will not be discussed in detail, but a few LDA results shall be used for qualitative considerations on the surface charge density distribution in order to explain elastic and inelastic HAS spectra.

3.3. *Phonons*

The energy of the ZA and LA/TA modes at $Q = 0$ ($\bar{\Gamma}$-point) have been estimated in an ab initio frozen-phonon scheme by rigidly displacing the graphene sheet either vertically or parallel to the substrate surface, respectively, while keeping the Ru atoms fixed. The phonon energies derived in this way are 23.7 meV for the ZA mode and 7.9 meV for the degenerate pair of LA and TA modes. This technique was tested by calculating the energies of the ZA mode for the Gr–Ni(111) (1×1) system, where the reconstruction is small enough to allow for a complete DFPT calculations. The results of this frozen-phonon technique were found to be in agreement within 6% with the more accurate DFPT results. With respect to a precise DFPT calculation the frozen-phonon method is expected to give stiffer frequencies, as it does not allow atoms to change the reciprocal positions during motion.

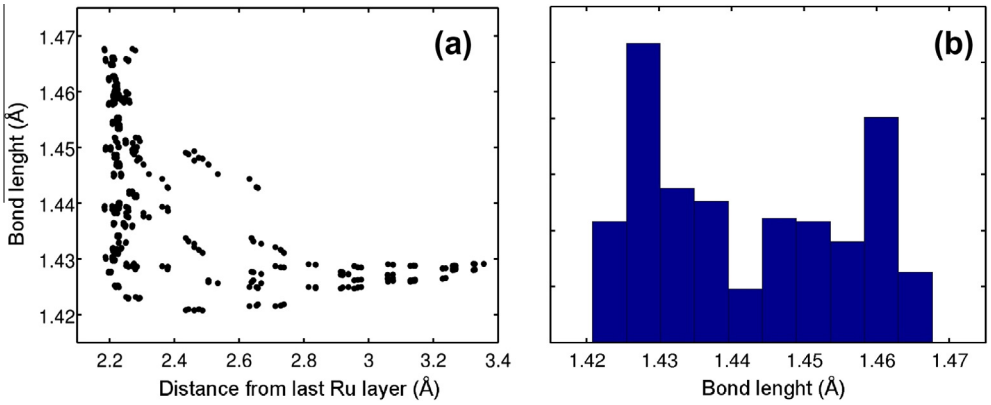

Fig. 5 – (a) Bond lenght in the graphene layer as a function of the height with respect to the last Ru plane. (b) Bond lenght distribution. (A colour version of this figure can be viewed online.)

A simple fit of the ZA and RW bands by a double linear chain model suggests for the ZA mode an energy of about 16 meV at Q = 0 (see green curves in Fig. 3). This value is close to the energy of 15.6 meV measured for the $Q_{\parallel} = 0$ breathing mode of the graphite bilayer [32], and corresponds to an effective Gr–Ru force constant 5 times stiffer than the interlayer force constant in graphite. However, considering that only part of the graphene layer is in close contact with the Ru surface due to the existence of bumps and valleys in the surface unit cell, the local force constant per unit area in the contact region must be considerably larger than in graphite. The double linear chain model reproducing the ZA dispersion of free-standing graphene and the RW dispersion of the Ru(0001) free surface is described by the equations:

$$\omega^2_{0,\mathrm{Gr}}(Q) = (F/2m_C)\sin^4(a_{\mathrm{Gr}}Q)[1+\alpha\sin^2(a_{\mathrm{Gr}}Q)]$$
$$\omega^2_{0,\mathrm{Ru}}(Q) = (f/m_{\mathrm{Ru}})\sin^2(a_{\mathrm{Ru}}Q), \quad (1)$$

with $F = 3.17\times10^{-20}$ meV^2/g and $f = 8.12\times10^{-20}$ meV^2/g the force constants appropriate to graphene and Ru(0001), $m_C = 12$ a.u. and $m_{\mathrm{Ru}} = 101$ a.u. the respective masses (there are two C masses for one Ru mass), a_{Gr} and a_{Ru} the periods of graphene and Ru(0001) in the chosen direction. The parameter α (here $\alpha = 5$) corrects the parabolic dispersion of graphene at small Q as in [26], so as to best fit the free-standing graphene dispersion. The two linear chains are then coupled through an interlayer force constant $g = 3.37\times10^{-20}$ meV^2/g (assumed to be independent of Q despite the 11-to-12 misfit of the two periods) so as to fit as well as possible the measured ZA and RW dispersion curves. In this operation it is also considered that the ZA and LA degrees of freedom are weakly coupled due to the fact that the graphene sheet is not a mirror plane as for the free-standing case. This yields an avoided crossing between the ZA and LA branches. The fit shown in Fig. 3 is obtained for a coupling force constant of 0.31×10^{-20} meV^2/g.

The sequence of low-energy data points located at ca. 3 meV all over the BZ was not previously observed, neither on Ru(0001) nor on the graphite surfaces. This mode, labeled as M in Fig. 3, is interpreted as due to umklapp scattering processes involving the small reciprocal vectors $\mathbf{g} = (m, 0)$ associated with the long corrugation period and leading to the moiré satellite peaks (*m*,0) in the diffraction spectrum (see Fig. 1). These data points are reminiscent of what recently observed with helium-3 spin-echo scattering in the $23\times\sqrt{3}$ reconstructed Au(111) surface, where the large period reconstruction allows for new branches of low-energy excitations known as phasons, which can have either acoustic or optical character [38]. Actually the lowest phason branch would originate from the avoided crossings at the folding points of the set of RW branches with origins at Q = *m*(1,0), *m*(2,0), etc. (the reciprocal vectors of the large-period moiré structure). However, the corresponding intensities should decrease with the intensity of the corresponding moiré peaks in the diffraction spectrum. Thus, an alternative explanation could be to associate the M modes to vertical oscillation of the domes, similar to the fundamental mode of a drum membrane. This would also lead to a low-lying branch with no dispersion, due to the negligible coupling between neighbour domes.

While the physics of the RW, ZA and LA modes is rather transparent, the observation of the S7 branch in Gr/Ru(0001) exactly where it was found in graphite (0001) poses the same unsolved problem already considered for the early HAS measurements. For one, the SH branch cannot be observed if the scattering plane is parallel to a crystallographic mirror-symmetry plane, which is the case of the current experiments. Even assuming that this symmetry is (weakly) broken by the substrate misfit and consequent formation of the periodically rippled reconstruction and the moiré pattern [17], a softening as large as 40% of the S7 surface branch with respect to its parent TA branch in graphite [33] would not be compatible with the small perturbation that the substrate, whether graphite or ruthenium, exerts on the graphene layer.

Since for incident energies below 1 eV the inelastic interaction of He atoms with the atoms of a conducting surface is always mediated by the conduction electrons [34], at the Fermi energy whose wavefunctions mostly extend outside the surface [31], it is natural to think that the energy released at the atom-surface inelastic collision is retained by the electron degrees of freedom in the form of low-energy excitations

(if any) rather then transmitted to the atomic degrees of freedom (phonons). The HAS scattering amplitudes are proportional to the Fourier transform of the electron density–density correlation function [31], and the inelastic amplitudes to the surface electron-density modulation produced by the elementary excitations of the surface. Among these, also low-energy plasmons (2D-plasmons, acoustic surface plasmons (ASP) [36]) can in principle be excited by HAS with a measurable intensity [37].

It comes however as a surprise the observation of the so-called S7 branch in close agreement with graphite, since no acceptable interpretation was found so far for that branch in graphite. The branch is too soft for being that of SH modes [39] and SH modes would be anyway forbidden for planar scattering in the $\overline{\Gamma}\overline{M}$ direction, as the one used in the present experiments. The attribution of the additional branch in graphite to various defects, suggested by Oshima et al. [39], is incompatible with the high quality of the surface, proved by the very small diffuse elastic peak in those early measurements. On the other hand, Oshima et al. HREELS data meet a similar difficulty showing around the M-point two distinctly separated peaks, whereas inelastic X-ray data [33] and theory [40] give a degenerate pair. Thus also HREELS gives an additional mode, although only near the M-point, whereas the signatures of the S7 mode along $\overline{\Gamma}\overline{M}$ are very weak, if any at all. A re-analysis of the old HAS data, including an unpublished series of measurements for a hot graphite surface (700 K) and larger incident energy (up to 110 meV), support the assumption that the S7 branch of graphite is not an artifact [41]. There is a wide theoretical literature on 2D-plasmons and ASPs in graphene [42], which however predicts dispersion curves considerably steeper than the present S7 branch, at least for reasonable values of the parameters involved. The same the EELS measurements of plasmon excitations in graphene with dispersion curves vanishing at zero momentum have apparently no connection with the S7 branch [44,45]. On the other hand, plasmonic excitation in the THz range have been reported from scanning tunneling spectroscopy (STS) [43], and magneto-plasmon spectroscopy [46] though with no hint about their dispersion.

3.4. *Static and dynamic surface charge densities*

The charge density profiles calculated along a straight line crossing the cell center for increasing values of the charge density are shown in Fig. 4 for both PBEGA (a) and LDA (b). The profile for the lowest density of 1×10^{-4} a.u. represents the classical turning point of He atoms at the incident energy used in our diffraction experiments. The PBEGA gives more reliable charge distributions but suffers from numerical noise, whereas LDA, allowing for a much smaller numerical noise even at the lowest densities, is known to give overbinding, which here means a larger corrugation and a smaller graphene–substrate distance. Both results, however, indicate that the long-period electronic corrugations probed by HAS at about 4 Å away from the C atoms (1.09 Å for PBEGA, 1.35 Å for LDA) is only slightly smaller than the respective atomic corrugations. A more evident smoothing of the electronic density for increasing distance from the C atoms occurs in the short-period corrugation.

In order to clarify the origin of the intense diffraction peaks associated with the Ru(0001) periodicity in the graphene-covered sample, calculations of the surface charge density have been performed with and without the Ru substrate, preserving in the latter case the same atomic corrugation of the graphene layer. It appears that the contribution of the Ru orbitals to the surface charge density perceived by the He atoms is quite small, as expected for the comparatively localized states of a d-metal surface and the modest charge transfer to graphene [24]. Despite the small contribution of the Ru orbitals to the surface charge density 4 Å above the Gr surface, the calculated LDA charge density map for a density as low as 4×10^{-5} a.u. (Fig. 6(a)) keeps bearing the information of Ru(0001) periodicity, as shown by the Fourier transform of the density profile along the $\overline{\Gamma}\overline{M}$ direction plotted in Fig. 6(b). Here the prominent diffraction features associated to both graphene (Gr) and ruthenium (Ru) periodicities, as well as the corresponding moiré (M) satellite peaks, are in evidence (despite the numerical noise) with relative intensities in agreement with

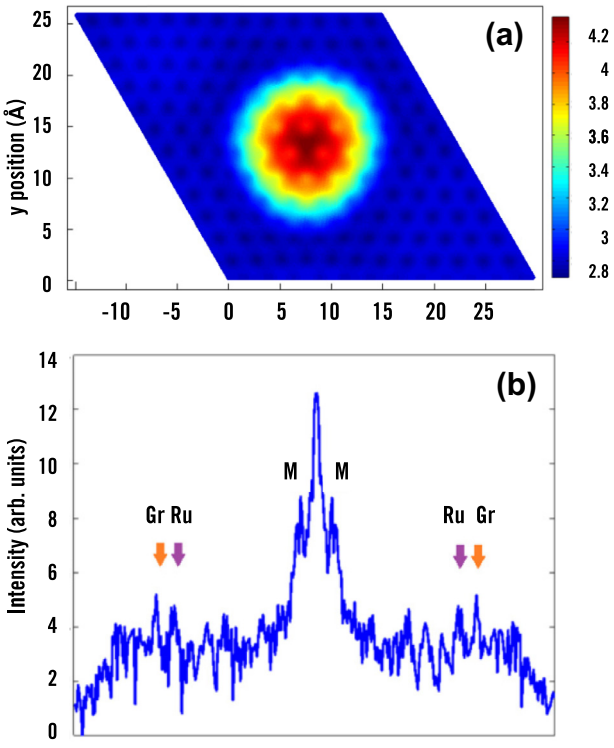

Fig. 6 – (a) LDA charge density map corresponding to a charge density of 4×10^{-5} a.u. at about 4 Å from a graphene monolayer on a 3ML Ru(0001) substrate. (b) Fourier transform of the charge density depicted in (a) along the $\overline{\Gamma}\overline{M}$ direction. Despite the numerical noise, the prominent diffraction features associated with graphene (Gr), ruthenium (Ru) and moiré (M) periodicities are cleary observed, in agreement with experiment (see Fig. 1). (A colour version of this figure can be viewed online.)

experiment. The persistence of signatures of Ru(0001) periodicity far above the graphene layer can only be attributed to the lateral relaxation of the carbon atoms so as to adapt as well as possible to the substrate periodicity, as also suggested by the bond-length distribution shown in Fig. 5.

A calculation of the surface charge density oscillation (SCDO) induced by the Ru RW displacement at $Q = \overline{M}$, keeping the graphene overlayer rigid, shows a modulation of the surface charge density profile for 1×10^{-5} a.u. which is quite distant from the the turning point profile (Fig. 7). An extrapolation to the turning point would give a SCDO of an order of magnitude smaller, less than 1% of the static charge density, whose calculation would yield a very noisy profile. This is however the order of magnitude of the SCDO at the turning point for the zone-boundary RW, calculated for a much simpler surface, Cu(111) [35]. Thus the actual SCDOs should be sufficient to explain the observed inelastic scattering intensity from Ru RW up to the zone boundary according to the quantum-sonar effect. This conclusion does not mean, however, that at large wavevectors the graphene layer remains at rest, as assumed in the SCDO calculation: the graphene layer, although almost rigidly, oscillates with the

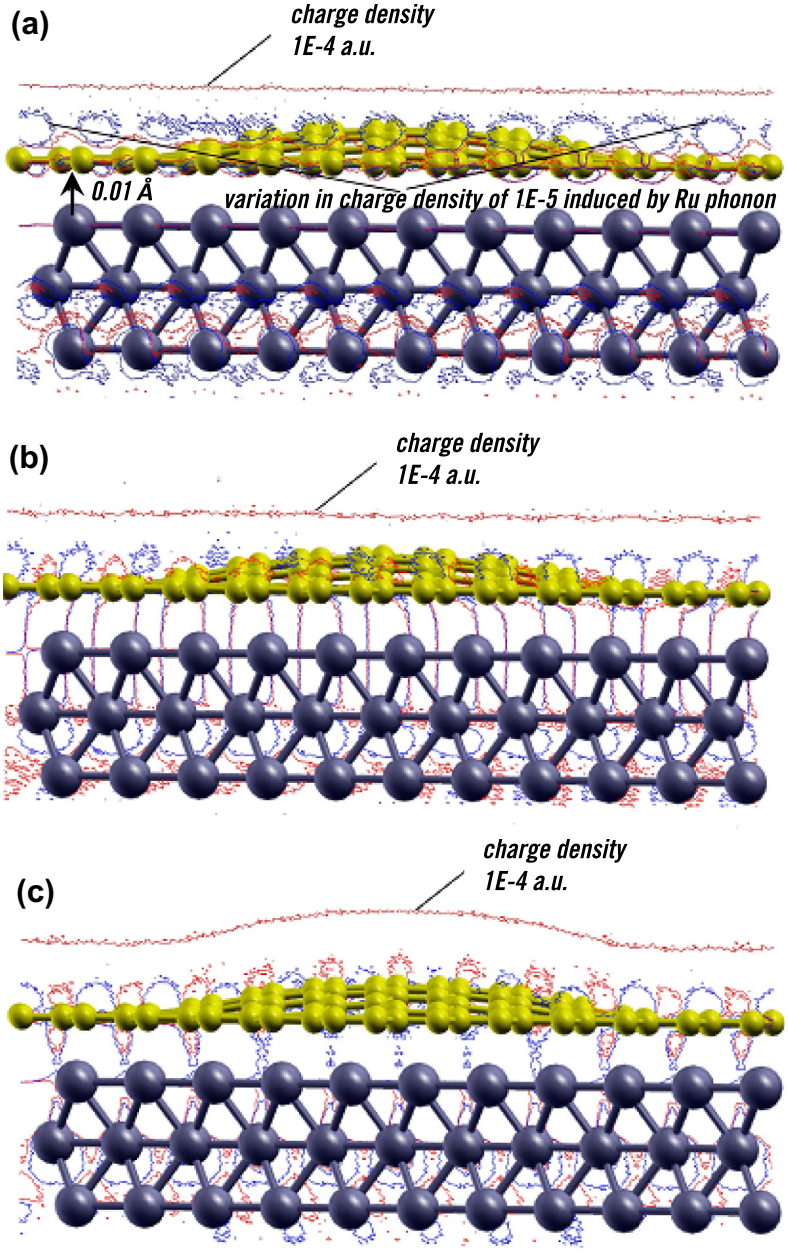

Fig. 7 – Charge density oscillation at the $\overline{M}$ point for different slices of the Gr/Ru(0001) unit cell: (0a) low region, (b) 1/4 of the cell, (c) 1/2 of the cell (top region). The continuous line above the graphene sheet is the static charge density profile at 1×10^{-4} a.u., approximately corresponding to the locus of turning points of He scattering. The charge density oscillation profiles at $+1 \times 10^{-5}$ a.u. (red contour lines) and -1×10^{-5} a.u. (blue contour lines) are calculated for an $\overline{M}$ point RW ± 0.01 Å oscillation of the surface Ru atoms alone. Calculations have been performed using the PBE + Grimme approximation. (A colour version of this figure can be viewed online.)

underlying Ru surface, as expected from the strong bonding to the substrate [16]. This is signalled by the fact that, when the graphene overlayer is added, the Ru(0001) RW branch is slightly softened at short wavelengths as an effect of loading. At the zone boundary the addition of 24 carbon masses to 11 Ru masses yields a clean-to-covered ratio of the RW energies of $(1399/1111)^{1/2} = 1.122$, in agreement with the experimental data extrapolated to the $\overline{M}$ point.

Our results provide an explanation for the surprisingly high reflectivity for neutral He and H_2 beams reported for the Gr/Ru(0001) surface [15]. Being the mass of the incoming He atoms and the C atoms on the graphene layer of similar order of magnitude, momentum transfer in the scattering process is expected to be very efficient, which should lead to the observation of a very low reflectivity, i.e., to a large Debye–Waller exponent. This is in contrast with the experimental observation of a reflectivity $\sim 23\%$ of the incoming intensity for He beams [15]. The removal of the (quasi-) parabolic dispersion of the ZA mode in graphene (graphite) and its replacement with the linearly dispersed RW almost identical to that present on clean Ru(0001) finally solves the riddle, and shows that it arises as the result of a strong C–Ru interaction. It also suggests that systems with a similar strong C–substrate interaction, like Gr/Ni(111), could also behave as excellent mirrors for He atoms.

4. Conclusions

In summary, we have presented a combined experimental and theoretical study of the acoustic phonon dispersion curves of graphene on Ru(0001). A quite interesting result is the observation of essentially the same Rayleigh mode on both clean Ru(0001) and Gr/Ru(0001) surfaces. DFT calculations show that this is due to the strong bonding and to the ability of HAS to detect subsurface phonons at short wavelengths, due to the induced surface-charge density oscillations. The fact the lowest observed branch is actually the substrate RW dispersion finally accounts for the observed very high reflectivity of Gr/Ru(0001) to He atoms, and suggests that systems with a strong C–Ru interaction are the best candidates to be used as focusing mirrors in scanning He atom microscopy [13]. Our data also provide evidence for the existence of a new acoustic branch, which cannot be ascribed to any phonon mode. It is hoped that the present finding, actually a confirmation that graphene on Ru(0001) behaves like graphite in giving an additional unexpected acoustic dispersion curve, will further stimulate the study of possible low-energy acoustic plasmon excitations in supported graphene.

Acknowledgements

We gratefully acknowledge J.P. Toennies and the Max-Planck-Gesellschaft for the donation of the scattering apparatus used in our experiments. This work has been supported by projects FIS 2013-40667-P, FrontNanoMagnet and by the European Union, FP7: Theme NMP.2012.1.4-3 Grant No. 309672.

REFERENCES

[1] Oshima C, Nagashima A. Ultra-thin epitaxial films of graphite and hexagonal boron nitride on solid surfaces. J Phys Condens Matter 1997;9:1.
[2] Shikin AM, Farías D, Adamchuk VK, Rieder KH. Surface phonon dispersion of a graphite monolayer adsorbed on Ni(111) and its modification caused by intercalation of Yb, La and Cu layers. Surf Sci 1999;424:155.
[3] Shikin AM, Farías D, Rieder KH. Phonon stiffening induced by copper intercalation in monolayer graphite on Ni(111). Europhys Lett 1998;44:44.
[4] Farías D, Shikin AM, Rieder KH, Dedkov YS. Synthesis of a weakly bonded graphite monolayer on Ni(111) by intercalation of silver. J Phys Condens Matter 1999;11:8453.
[5] Farías D, Rieder KH, Shikin AM, Adamchuk VK, Tanaka T, Oshima C. Modification of the surface phonon dispersion of a graphite monolayer adsorbed on Ni(111) caused by intercalation of Yb, Cu and Ag. Surf Sci 2000;454:437.
[6] Yan JA, Ruan WY, Chou MY. Phonon dispersions and vibrational properties of monolayer, bilayer, and trilayer graphene: density-functional perturbation theory. Phys Rev B 2008;77:125401.
[7] Lindsay L, Broido DA, Mingo N. Flexural phonons and thermal transport in graphene. Phys Rev B 2010;82:115427.
[8] Nika DL, Balandin AA. Two-dimensional phonon transport in graphene. J Phys Condens Matter 2012;24:233203.
[9] Ong ZY, Pop E. Effect of substrate modes on thermal transport in supported graphene. Phys Rev B 2011;84:075471.
[10] Amorin B, Guinea F. Flexural mode of graphene on a substrate. Phys Rev B 2013;88:115418.
[11] Aizawa T, Souda R, Otani S, Ishizawa Y, Oshima C. Bond softening in monolayer graphite formed on transition-metal carbide surfaces. Phys Rev B 1990;42:11469.
[12] Farías D, Rieder K. Atomic beam diffraction from solid surfaces. Rep Progr Phys 1998;61:1575.
[13] Holst B, Allison W. An atom-focusing mirror. Nature 1997;390:244;
Koch M, Rehbein S, Schmahl G, Reisinger T, Bracco G, Ernst WE, et al. Imaging with neutral atoms: a new matter-wave microscope. J Microsc 2008;229:1.
[14] Politano A, Borca B, Minniti M, Hinarejos JJ, Vázquez de Parga AL, Farías D, et al. Helium reflectivity and Debye temperature of graphene grown epitaxially on Ru(0001). Phys Rev B 2011;84:035450.
[15] Sutter P, Minniti M, Albrecht P, Farías D, Miranda R, Sutter E. A high-reflectivity, ambient-stable graphene mirror for neutral atomic and molecular beams. Appl Phys Lett 2011;99:211907.
[16] Vázquez de Parga AL, Calleja F, Borca B, Passeggi MCG, Hinarejos JJ, Guinea F, et al. Periodically rippled graphene: growth and spatially resolved electronic structure. Phys. Rev. Lett. 2008;100:056807.
[17] Borca B, Barja S, Garnica M, Minniti M, Politano A, Rodriguez-García JM, et al. Electronic and geometric corrugation of periodically rippled, self-nanostructured graphene epitaxially grown on Ru(0001). New J Phys 2010;12:093018.
[18] Ernst HJ, Hulpke E, Toennies JP. Helium-atom-scattering study of the structure and phonon dynamics of the W(001) surface between 200 and 1900 K. Phys Rev B 1992;46:16081.
[19] Barredo D, Laurent G, Nieto P, Farías D, Miranda R. High-resolution elastic and rotationally inelastic diffraction of D2 from NiAl(110). J Chem Phys 2010;133:124702.
[20] Braun J, Kostov KL, Witte G, Surnev L, Skofronick JG, Safron SA, et al. Surface phonon dispersion curves for a hexagonally close packed metal surface: Ru(0001). Surf Sci 1997;372:144.

[21] Perdew JP, Burke K, Ernzerhof M. Generalized gradient approximation made simple. Phys Rev Lett 1996;77:3865.
[22] Giannozzi P et al. QUANTUM ESPRESSO: a modular and open-source software project for quantum simulations of materials. J Phys Condens Matter 2009;21:395502. www.quantum-espresso.org.
[23] Vanderbilt D. Soft self-consistent pseudopotentials in a generalized eigenvalue formalism. Phys Rev B 1990;41:7892.
[24] Stradi D, Barja S, Díaz C, Garnica M, Borca B, Hinarejos J, et al. Role of dispersion forces in the structure of graphene monolayers on ru surfaces. Phys Rev Lett 2011;106:186102.
[25] Iannuzzi M, Kallchava I, Ma H, Leake SJ, Zhou H, Li G, et al. moiré beatings in graphene on Ru(0001). Phys Rev B 2013;88:125433.
[26] Karssemeijer LJ, Fasolino A. Phonons of graphene and graphitic materials derived from the empirical potential LCBOPII. Surf Sci 2011;605:1611.
[27] Minniti M, Díaz C, Fernández Cuñado JL, Politano A, Maccariello D, Martín F, et al. Helium, neon and argon diffraction from Ru(0001). J Phys Condens Matter 2012;24:354002.
[28] Mounet N, Marzari N. First-principles determination of the structural, vibrational and thermodynamic properties of diamond, graphite, and derivatives. Phys Rev B 2005;71:205214.
[29] Smilgies DM, Toennies JP. Resolution and intensity considerations of an ideal He atom timeofflight spectrometer for measurements of surface phonon dispersion curves. Rev Sci Instrum 1988;59:2185.
[30] Benedek G, Brusdeylins G, Heimlich C, Toennies JP, Valbusa U. Surface phonons in graphite (001). Surf Sci 1986;178:545.
[31] Benedek G, Bernasconi M, Bohnen KP, Campi D, Chulkov EV, Echenique PM, et al. Unveiling mode-selected electronphonon interactions in metal films by helium atom scattering. Phys Chem Chem Phys 2014;16:7159.
[32] Nicklow R, Wakabayashi N, Smith HG. Lattice dynamics of pyrolytic graphite. Phys Rev B 1972;5:4951.
[33] Mohr M, Maultzsch J, Dobard E, Reich S, Milo I, Damnjanovi M, et al. Phonon dispersion of graphite by inelastic X-ray scattering. Phys Rev B 2007;76:035439.
[34] Sklyadneva IY, Benedek G, Chulkov EV, Echenique PM, Heid R, Bohnen KP, et al. Mode-selected electron–phonon coupling in superconducting Pb nanofilms determined from He atom scattering. Phys Rev Lett 2011;107:095502.
[35] Chis V, Hellsing B, Benedek G, Bernasconi M, Chulkov EV, Toennies JP. Large surface charge density oscillations induced by subsurface phonon resonances. Phys Rev Lett 2008;101:206102. Erratum: Phys Rev Lett 2009;103:069902.
[36] Diaconescu B et al. Low-energy acoustic plasmons at metal surfaces. Nature (London) 2007;448:57.
[37] Benedek G, Pardo M, Toennies JP. Theory of inelastic atom scattering from surface electron-hole and plasmon excitations in highlights on spectroscopies of semiconductors and nanostructures. In: Guizzetti G, Andreani AC, Marabelli F, Patrini M, editors. Conf. Proc., vol 94. SIF, Bologna; 2007. p. 151.
[38] McIntosh EM, Kole PR, El-Batanouny M, Chisnall DM, Ellis J, Allison W. Measurement of the phason dispersion of misfit dislocations on the Au(111) surface. Phys Rev Lett 2013;110:086103.
[39] Oshima C, Aizawa T, Souda R, Ishizawa Y, Sumiyoshi Y. Surface phonon dispersion curves of graphite (0001) over the entire energy region. Solid State Commun 1988;65:1601.
[40] Maultzsch J, Reich S, Thomsen C, Requardt H, Ordejón P. Phonon dispersion in graphite. Phys Rev Lett 2004;92:075501.
[41] Brusdeylins G. Private communication.
[42] Das Sarma S, Qiuzi Li. Intrinsic plasmons in two-dimensional Dirac materials. Phys Rev B 2013;87:235418;
Bostwick A et al. Observation of plasmarons in quasi-freestanding doped graphene. Science 2010;328:999;
Grigorenko AN, Polini M, Novoselov KS. Graphene plasmonics. Nat Photon 2012;6:749;
Pisarra M et al. Acoustic plasmons in extrinsic free-standing graphene. New J Phys 2014;16:083003.
[43] Vitali L, Schneider MA, Kern K, Wirtz L, Rubio A. Phonon and plasmon excitation in inelastic electron tunneling spectroscopy of graphite. Phys Rev B 2004;69:121414R.
[44] Politano A, Chiarello G. Emergence of a nonlinear plasmon in the electronic response of doped graphene. Carbon 2014;71:176.
[45] Politano A, Marini A, Chiarello G. Effects of a humid environment on the sheet plasmon resonance in epitaxial graphene. Phys Rev B 2012;86:085420.
[46] Crassee M, Orlita, Potemski M, Walter AL, Ostle M, Seyller TL, et al. Intrinsic terahertz plasmons and magnetoplasmons in large scale monolayer graphene. Nano Lett 2012;12:2470.